Anisotropic Zeeman splitting in semimagnetic quantum-well structures

D. Suisky
Institut für Physik, Humboldt-Universität zu Berlin, Invalidenstrasse 110, D-10115 Berlin, Germany

W. Heimbrodt
Fachbereich Physik und Zentrum für Materialwissenschaften, Philipps-Universität Marburg, Renthof 5, D-35032 Marburg, Germany

C. Santos, F. Neugebauer, and M. Happ
Institut für Physik, Humboldt-Universität zu Berlin, Invalidenstrasse 110, D-10115 Berlin, Germany

B. Lunn, J. E. Nicholls, and D. E. Ashenford
Department of Applied Physics and Engineering, Design and Manufacture, University of Hull, Hull HU6 7RX, United Kingdom
(Received 12 March 1998)

The Zeeman splitting pattern in semimagnetic superlattices and asymmetric double quantum wells composed of different sequences of semimagnetic and nonmagnetic well and barrier materials have been investigated experimentally and theoretically, in particular, in dependence on the orientation of an external magnetic field and the lattice mismatch induced biaxial strain. The magneto-optical anisotropy, which appears by varying the tilting angle of the magnetic field, can be explained by coupling of heavy- and light-hole states of the Γ_8 valence band. Theoretical results have been obtained by transfer matrix method and are compared with experimental photoluminescence and photoluminescence excitation spectra obtained on superlattices and asymmetric double quantum wells. [S0163-1829(98)10931-1]

I. INTRODUCTION

Diluted magnetic semiconductors (DMS's) are ternary or quaternary alloys where the incorporated magnetic ions have a direct and important effect on a variety of optical and transport properties. One of these properties, the so called ''giant Zeeman effect'' has encouraged intense research activity on this group of materials. The splitting of the order of 100 meV is caused by the interaction between the localized spins of manganese ions and the spins of electrons and holes of the host material (usually referred to as s,p-d exchange interaction). The most extensively studied materials are the $(A_{II}Mn)B_{VI}$ alloys.[1,2]

The fabrication of dimensionally reduced DMS quantum-well (QW) structures is providing a most powerful tool for the investigation of large variations of carrier confinement energies and their influence on optical and transport properties in one and the same sample. Such investigations require in most cases the preparation of a series of samples differing from each other in the alloy composition.

However, the symmetry reduction of the cubic zinc-blende quantum-well structures (which is caused by the quasi-2D layer structure and the internal strain induced by the lattice mismatch of different materials) yields a splitting of the zone center heavy-hole (HH) and light-hole (LH) valence-band states. Hence, the orientation of the magnetic field has to be related to the symmetry axis and a magneto-optical anisotropy has been observed strongly enhanced by DMS constituents of the structures.[3–6]

The investigations of the magneto-optical anisotropy have been concentrated preferentially on configurations where the magnetic field is oriented either parallel (Faraday configuration) or perpendicular (Voigt configuration) to the growth direction.[3–6] Tilted field configurations are only rarely investigated.[3] The observed magneto-optical anisotropy in single quantum wells (SQW's) was qualitatively explained by the different orientation of the magnetic-field direction relative to the confined quasi-2D exciton in the quantum well.[3] The role of the band-structure anisotropy has been analyzed by Peyla *et al.*[5] on excitonic transitions in SQW's consisting of nonmagnetic material in between DMS barriers. The splitting pattern in Voigt configuration was explained by the anisotropy of the band structure that causes a coupling of HH and LH states by finite momentum.

In this paper we will study superlattices (SL's) and asymmetric double quantum wells (ADQW's) composed of different sequences of DMS and nonmagnetic materials where either the barriers or the wells consist of DMS material. We give a theoretical approach, where the LH-HH coupling is mediated by the magnetic field itself and is strongly enhanced by the s,p-d exchange interaction. The model includes lattice mismatch induced internal strain and is not restricted to the preferential orientations of the magnetic field in either Faraday or in Voigt geometry but includes also all intermediate orientations of the magnetic field on equal footing. It accounts therefore directly for tilted field configurations. We study structures based on $CdTe/Cd_{1-x}Mn_xTe$ and $Zn_{1-x-y}Cd_yMn_xSe/ZnSe$ theoretically and experimentally and explain the spectra by the giant Zeeman splitting. Other magnetic field correlated effects as the usual Zeeman splitting or the Landau-level splitting are at least one order of magnitude below the effects due to the exchange interaction and have not been observed, therefore, in the experimental spectra of wide-gap bulk DMS's nor in our experiments on DMS QW's.

The paper is organized as follows. In the next section we

discuss the model that describes the band structure and the influence of the magnetic field and the strain in the framework of the effective-mass approximation (EMA). In Sec. III we give a short summary of the transfer matrix method and the envelope function approximation and their application to heterostructures. In Sec. IV we study the magneto-optical anisotropy in various types of DMS structures such as SL's, SQW's, and ADQW's. We discuss the dependence of the magneto-optical anisotropy on geometrical and material parameters and compare our theoretical results with experimental data.

II. HAMILTONIAN OF SEMIMAGNETIC BULK MATERIAL

Semiconductor heterostructures are most commonly described as a sequential arrangement of layers of different semiconducting materials, where each of the layers is assumed to have bulk properties.

The Hamiltonian for DMS materials can be written in the form

$$H=\sum_{\nu=c,v}(H^{\nu}_{cryst}+H^{\nu}_{str}+H^{\nu}_{zee}+H^{\nu}_{exc}), \tag{1}$$

where H_{cryst} is the Bloch Hamiltonian of the bulk and H_{str} includes the strain in the material caused by the lattices mismatch of different materials. H_{zee} describes the interaction of Bloch electrons with an external magnetic field leading to the usual linear Zeeman splitting pattern. The last term H_{exc} describes the specific properties of DMS materials due to the s,p-d exchange interaction between the spin of Bloch electrons and the spin of the localized incorporated paramagnetic Mn ions. Considering the Γ_6 conduction band c and the Γ_8 valence-band complex v the index ν has to be specified to both these bands.

The magnetic-field-dependent contributions that follow from Eq. (1) for the conduction band for the magnetic field oriented parallel to the z axis in cubic materials can be summed up as follows:[7,8]

$$E=(l+\tfrac{1}{2})\hbar\omega_c\pm\tfrac{1}{2}(g_e\mu_B B-a(x_{\mathrm{Mn}})x_{\mathrm{Mn}}N_o\alpha\langle S_z(\vec{\mathbf{B}})\rangle). \tag{2}$$

The first term describes the Landau-level splitting. The second term describes the usual Zeeman splitting and the third contribution appears due to the exchange interaction. ω_c is the cyclotron frequency, μ_B is the Bohr magneton, and g_e is the electron Landé factor. x_{Mn} is the manganese concentration. $a(x_{\mathrm{Mn}})$ has been introduced as an additional fitting parameter that accounts for the clustering of Mn spins and the subsequent reduction of giant Zeeman splitting. For the same reasons the Curie-Weiss parameter $T_o(x_{\mathrm{Mn}})$ has been introduced into the argument $\xi=\frac{5}{2}g\mu_B B/\{k[T+T_o(x_{\mathrm{Mn}})]\}$ of the Brillouin function B_S in $\langle S_z(\vec{\mathbf{B}})\rangle=SB_S(\xi)$, which gives the averaged spin value in the framework of the mean-field approximation. $g\approx 2$ is the effective Landé factor and S is the total angular momentum. The parameter $N_o\alpha$ characterizes the strength of the exchange interaction and has to be taken from experiment. N_0 is the number of unit cells per unit volume.

The last term of Eq. (2) is the entirely dominant part in the experimental spectra obtained on the investigated $CdTe/Cd_{1-x}Mn_xTe$ and $Zn_{1-x-y}Cd_yMn_xSe/ZnSe$ QW structures. The reason is, that in DMS materials the energy $\hbar\omega_c$ and the usual Zeeman contribution are orders of magnitude smaller than the exchange splitting. The same arguments hold for the valence band complex, where the exchange interaction $N_o\beta$ is even stronger, e.g., $|N_o\beta|\approx 4|N_o\alpha|$ for $Cd_{1-x}Mn_xTe$ and $|N_o\beta|\approx 5|N_o\alpha|$ for $Zn_{1-x}Mn_xSe$.

Expanding H_{exc} in Eq. (1) into Kohn-Luttinger functions, we obtain for arbitrary orientation of the magnetic field (i) for the conduction band the 2×2 matrix,

$$H^{c}_{mag}=\begin{pmatrix} \frac{1}{2}G^{c}_{eff,z} & \frac{1}{2}(G^{c}_{eff,y}+iG^{c}_{eff,x}) \\ \frac{1}{2}(G^{c}_{eff,y}-iG^{c}_{eff,x}) & -\frac{1}{2}G^{c}_{eff,z}\end{pmatrix}, \tag{3}$$

with

$$(G^{c}_{eff,x},G^{c}_{eff,y},G^{c}_{eff,z})=a(x_{\mathrm{Mn}})x_{\mathrm{Mn}}\langle S(\vec{\mathbf{B}})\rangle N_0\alpha\vec{\mathbf{B}}/|\vec{\mathbf{B}}|;$$

and (ii) for the valence band the 4×4 matrix,

$$H^{v}_{mag}=\begin{pmatrix} \frac{3}{2}\delta & \gamma & 0 & 0 \\ \gamma^* & \frac{1}{2}\delta & \lambda & 0 \\ 0 & \lambda^* & -\frac{1}{2}\delta & \gamma \\ 0 & 0 & \gamma^* & -\frac{3}{2}\delta\end{pmatrix}, \tag{4}$$

where

$$\lambda=i(G^{v}_{eff,x}+iG^{v}_{eff,y}),\quad \gamma=i\frac{\sqrt{3}}{2}\lambda,\quad \delta=G^{v}_{eff,z}, \tag{5}$$

with

$$(G^{v}_{eff,x},G^{v}_{eff,y},G^{v}_{eff,z})=a(x_{\mathrm{Mn}})x_{\mathrm{Mn}}\langle S(\vec{\mathbf{B}})\rangle N_0\beta\vec{\mathbf{B}}/|\vec{\mathbf{B}}|.$$

III. ENVELOPE FUNCTION FOR HETEROSTRUCTURES AND TRANSFER MATRIX METHOD

In this section we shortly review the transfer matrix method for heterostructures within the envelope function approximation.[9–12] The wave function of the heterostructure in each layer in the vicinity of the Γ point may be expanded into the Bloch functions $u_{l,\nu}(\vec{r})$,

$$\Psi_{\nu}(\vec{r})=\sum_{l=1}^{n_\nu}F_{l,\nu}(z)u_{l,\nu}(\vec{r})e^{\imath k_x x}e^{ik_y y}, \tag{6}$$

where $n_c=2$ and $n_v=4$ indicate the degree of degeneracy of the conduction band $\nu=c$ and the valence-band $\nu=v$ states, respectively. The z axis is chosen parallel to the growth direction being crystallographically the [001] direction of the investigated heterostructures. The variables k_x and k_y denote the components of the two-dimensional wave vector $\vec{k}_\perp\equiv(k_x,k_y)$ that lies in the $\{x,y\}$ plane perpendicular to the growth direction of the heterostructures. Replacing k_z by $-i(\partial/\partial z)$ the envelope function $F_{l,\nu}(z)$ has to be calculated from the Schrödinger equation,

$$\sum_{l=1}^{n_\nu}\left[H^{\nu}_{ll'}\left(\vec{k}_\perp,-i\frac{\partial}{\partial z}\right)+U^{\nu}(z)\,\delta_{ll'}\right]F_{l,\nu}(z)=\varepsilon F_{l',\nu}(z), \tag{7}$$

where $H_{ll'}$ is the Kohn-Luttinger representation of the Hamiltonian in Eq. (1). $U(z)$ denotes the quantum-well potentials that result from the band offsets between the various materials the heterostructure is made of. The Hamiltonian in Eq. (7) may be rewritten in terms of powers of $-i(\partial/\partial z)$,

$$\sum_{l=1}^{n_\nu}\left[-A^{\nu}_{ll'}\frac{\partial^2}{\partial z^2}-iB^{\nu}_{ll'}\frac{\partial}{\partial z}+C^{\nu}_{ll'}(z)\right]F_{l,\nu}(z)=\varepsilon F_{l',\nu}(z), \tag{8}$$

where the matrices A, B, and C follow from Eq. (7). The matrix A consists only of diagonal elements originating from the Hamiltonian H_{cryst} in Eq. (1) and is independent of the components of the vector $\vec{\mathbf{k}}_\perp$ whereas the matrices B and C depend, in general, on those components. In PL experiments only excitonic transitions near the Γ point are observed. In terms of the wave vectors of electron and hole it follows from the vertical transition selection rule $\vec{\mathbf{k}}_\mathbf{e}=\vec{\mathbf{k}}_\mathbf{h}=0$. Therefore, one can set $k_x=k_y=0$ in H_{kp} in Eq. (1) and all elements of the matrix B vanish. Equations (6) to (8) together with appropriate boundary conditions[11] enable the calculation of eigenvalues and eigenfunctions of heterostructures with layers of arbitrary thickness, shape and material. In the case of an SL one needs to consider additionally the periodicity along the superlattice axis. For any nonperiodic finite QW structure one has to select those wave functions that vanish at infinity. In order to solve the eigenvalue problem in Eq. (8) numerically by transfer matrix method, we introduce the vector $\vec{\Phi}(z)$

$$\vec{\Phi}(z)=\left[F_1(z),F_2(z),\ldots,F_{n_\nu}(z),\ \frac{\partial F_1(z)}{\partial z},\frac{\partial F_2(z)}{\partial z},\ldots,\frac{\partial F_{n_\nu}(z)}{\partial z}\right], \tag{9}$$

and obtain the following solutions for periodic and nonperiodic structures:

a. Superlattices. Due to periodicity along the z axis we have to fulfill

$$\vec{\Phi}(z+d)=\exp(iqd)\vec{\Phi}(z), \tag{10}$$

where d is the period of the superlattice and q denotes the corresponding wave vector. For a superlattice made of two different materials labeled 1 and 2 one obtains the equation

$$[J_{1,2}T_2J_{2,1}T_1-\exp(iqd)]\vec{\Phi}(z)=\vec{0}, \tag{11}$$

where the T_j and $J_{i,j}$ are the transfer matrices and the matching matrices, respectively. Nontrivial solutions of Eq. (11) are found from the vanishing determinant

$$\mathrm{Det}[J_{1,2}T_2J_{2,1}T_1-\exp(iqd)]=0. \tag{12}$$

b. Multiple quantum wells. Let us consider an MQW consisting of a material forming a large barrier on the left side labeled 1, a sequence of well-barrier regions of materials labeled $2,3,\ldots,m-1$ of thicknesses d_2,d_3,d_{m-1}, and a right barrier region of material m.

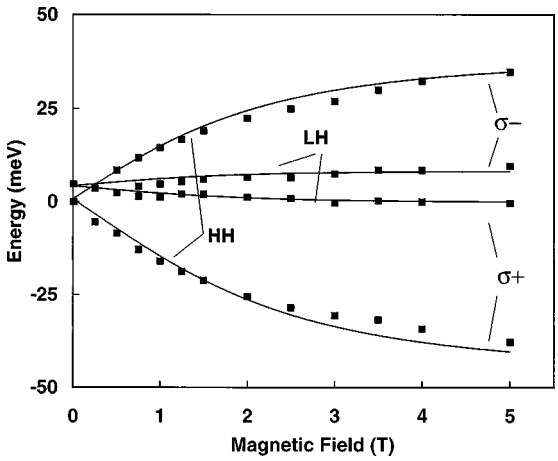

FIG. 1. Giant Zeeman splitting of HH and LH excitonic states for a CdTe/$Cd_{1-x}Mn_x$Te SL measured by PLE as a function of applied magnetic field in Faraday configuration ($\vec{\mathbf{B}}\|\mathbf{z}$). Parameters of the structure: well width $L_w=20$ Å, barrier width $L_b=20$ Å, $x_{\mathrm{Mn}}=0.21$, 400 wells. σ^+ and σ^- indicate the polarization state of the incident light. Full squares, experimental points. The curves are calculated. Parameters are given in the text.

The energy eigenvalues of MQW structures are to be calculated then from

$$\mathrm{Det}[J'_{m,m-1}T_{m-1}J'_{m-1,m-2}T_{m-2}\cdots J'_{3,2}T_2J_{2,1}U_L-U_R]=0, \tag{13}$$

where $J'_{i,j}$ are matching matrices as before and U_L and U_R are vectors resulting from the condition of vanishing wave functions at infinity.

IV. RESULTS AND DISCUSSION

In this section we discuss the magneto-optical properties of different types of SL's and QW's. In particular, we consider the dependence on strength and orientation of the magnetic field. Experimentally, the anisotropy of the valence-band splitting caused by the magnetic field can be proved by measurements of the corresponding excitonic transitions. The specimens were investigated by PL and PLE in an external magnetic field up to 7.5 T at 1.8 K. Tunable dye lasers with appropriate spectral ranges pumped by an Ar^{2+} laser were used as excitation sources and a grating spectrometer equipped with a charge-coupled device camera system was on the detection side.

A. Multiple quantum wells and superlattices

The experimentally observed splitting of the lowest HH and LH exciton in dependence on the magnetic-field strength are depicted in Figs. 1 and 2 by black squares for the well transitions of a strained semimagnetic CdTe/$Cd_{1-x}Mn_x$Te SL. The structure consists of 400 wells with a width of $L_w=20$ Å separated by barriers of $L_b=20$ Å. The wells are nonmagnetic. The Mn content in the barriers is $x_{\mathrm{Mn}}=0.21$. The samples were grown by MBE on InSb at a substrate temperature of 240 °C and a growth rate of 0.7 μm/h. In

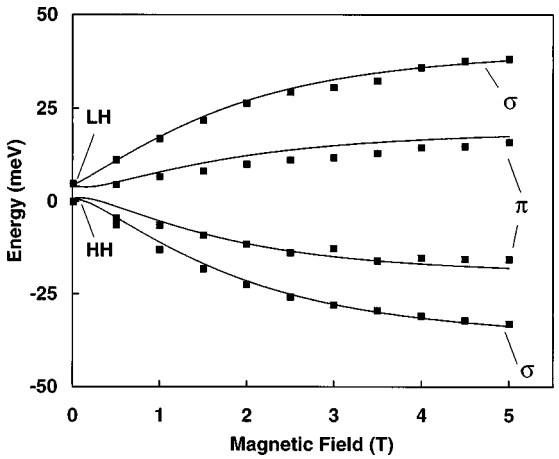

FIG. 2. Same as Fig. 1 but for Voigt configuration ($\vec{\mathbf{B}}\perp\mathbf{z}$).

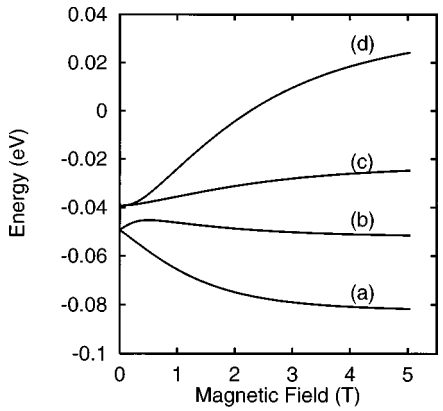

FIG. 3. Valence-band Zeeman splitting pattern vs magnetic-field strength for a CdTe/$Cd_{1-x}Mn_xTe$ SL in Voigt configuration. Parameters of the structure: nonmagnetic well, well width $L_w=20$ Å; DMS barrier, $x_{\mathrm{Mn}}=0.22$, barrier width $L_b=30$ Å.

Fig. 1 we show the experimental points and the calculated curves for Zeeman splitting in Faraday configuration ($\vec{\mathbf{B}}$ parallel to the growth direction, to the incident light propagation as well as the observation direction) and in Fig. 2 the corresponding Zeeman splitting in Voigt configuration with in-plane field ($\vec{\mathbf{B}}$ perpendicular to growth direction, incident light propagation and the observation direction). The energy gap of the barrier material is determined by the relation $E_{gap}=(1.605+1.59x_{\mathrm{Mn}})$ eV and the lattice constant is obtained from the relation $a_{\mathrm{Cd}_{1-x}\mathrm{Mn}_x\mathrm{Te}}=(6.481-0.146x_{\mathrm{Mn}})$ Å. The valence-band offset is assumed to be 33% of the total offset.[13] The effective HH and LH masses are calculated from the Luttinger parameters $\gamma_1=5.29$ and $\gamma_2=1.89$ (Ref. 14) to be $m_{hh}=0.662m_o$ and $m_{lh}=0.11m_o$.[14,15] The effective mass of the electron is $m_e=0.098m_o$.[16] The parameters of $Cd_{1-x}Mn_xTe$ are assumed to be approximately the same as for CdTe. The exchange integrals $N_o\alpha=0.22$ eV and $N_o\beta=-0.88$ eV are taken from Ref. 17. The only fitting parameters are the effective Mn concentration $a(x_{\mathrm{Mn}})$ and the Curie-Weiss-Parameter $T_o(x_{\mathrm{Mn}})$ which account for the Mn clustering and the Mn-Mn superexchange interaction as well as for the interface disorder of the DMS layers. The latter is known to have a strong influence on the paramagnetic properties. The calculated curves are in excellent agreement with the experimental data. It must be mentioned, however, that the parameters $a(x_{\mathrm{Mn}})$ and $T_o(x_{\mathrm{Mn}})$ also cover a small change of the exciton binding energy ϵ_{bind} with increasing field. ϵ_{bind} was calculated at zero field after Leavitt and Little[18] and kept constant for all field strengths as well as for both field directions. We expected, at least, a small difference of ϵ_{bind} for $\vec{\mathbf{B}}\|\mathbf{z}$ and $\vec{\mathbf{B}}\perp\mathbf{z}$ at highest field strengths. There was, however, no need to include such a difference into the fitting procedure.

The pronounced differences in the shape of the curves and in the magnitude of the splitting between Faraday and Voigt configuration shown in Fig. 1 and Fig. 2, respectively, are well reproduced by our model. (i) Instead of the crossing in Faraday configuration (see Fig. 1) an anticrossing of the curves appears in the splitting pattern in Voigt configuration (see Fig. 2), which is typically for interacting states. (ii) The splitting of the HH doublet in Voigt configuration is drastically reduced (the assignment is chosen as before with respect to the zero-field type of the states) whereas the LH splitting is enhanced.

These characteristic features of the magnetic-field dependence have been also observed for other types of SL's and QW structures, e.g., ZnSe/(Zn,Mn)Se (Ref. 19) or (Zn,Cd,Mn)Se/ZnSe (Ref. 20) and (Cd,Mn)Te/(Cd,Mg)Te.[6]

The origin of the observed anisotropy can be revealed by analyzing the type of wave functions belonging the different states in the splitting pattern. The conduction-band splitting pattern is independent of the orientation of the magnetic field and has to be ruled out. The origin can be found, however, by examining the valence-band envelope function. In Fig. 3 the magnetic field dependence of the HH and LH splitting pattern of the Γ_8 valence-band complex is shown that appears in the presence of confinement or the strain-induced HH-LH zero-field splitting. The curves are calculated for a CdTe/$Cd_{1-x}Mn_xTe$ SL. We may write the z-dependent part of the wave function $\Psi_\nu(\vec{r})$ in Eq. (6) in terms of the envelope functions $F_m^k(z)$ and the Kohn-Luttinger functions $|m\rangle$ $(m=-3/2,-1/2,+1/2,+3/2)$ for the Γ point in the general form

$$\phi_{\Gamma_8}^k(z)=F_{3/2}^k(z)|3/2\rangle+F_{1/2}^k(z)|1/2\rangle+F_{-1/2}^k(z)|-1/2\rangle+F_{-3/2}^k(z)|-3/2\rangle, \tag{14}$$

where $k=a,b,c,d$ indicate the energetically different states in the Zeeman pattern of the valence-band complex (see Fig. 3). The F_m^k are complex functions of the coordinate z and the magnetic field $\vec{\mathbf{B}}$. We visualize the character of the states by looking for the weighting factors of the expectation value of the four components $A_m^k(B)=\int dz|F_m^k(z)|^2$, for each state. In Faraday configuration, for any given field strength and energy $E(B)$ the envelope function is rather simple: the states belong to different m, and only one of the four components $|F_m^k(z)|^2$ gives a nonzero contribution to the envelope function. The state is then characterized entirely by the corresponding quantum number m and the normalized weighting factors do not change with the magnetic field. In Voigt configuration, the envelope functions are more complicated and are made up of all contributions belonging to different mag-

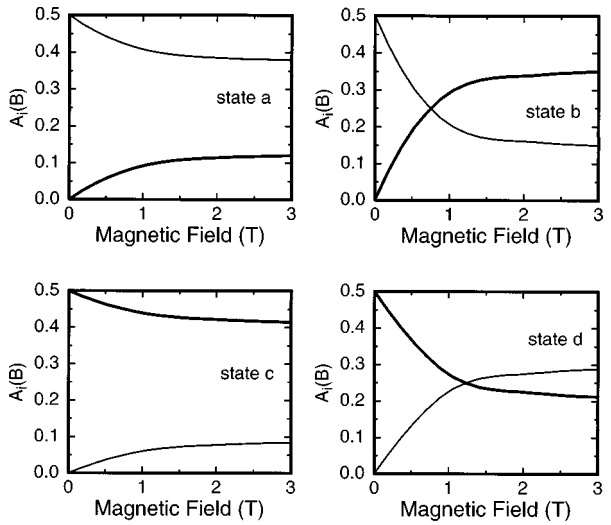

FIG. 4. Weighting factors of the $m=+3/2$ (thick line) and $m=+1/2$ (thin line) component of the envelope function belonging to the states (a) to (d) of Fig. 3.

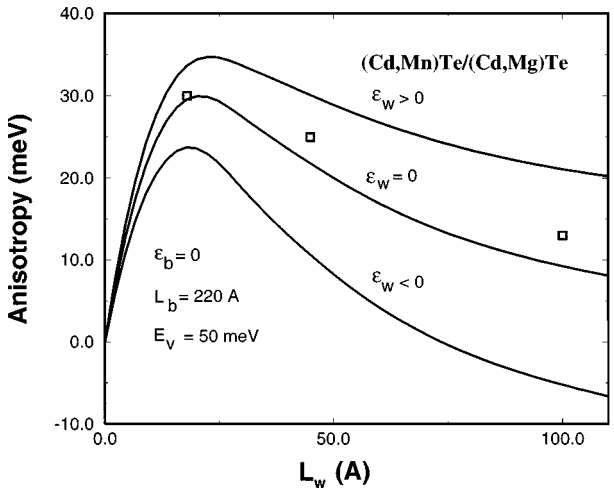

FIG. 5. Anisotropy of the Zeeman splitting pattern between Faraday and Voigt configuration in dependence on the barrier width in strained $Cd_{1-x}Mn_xTe/Cd_{1-x}Mg_xTe$ MQW structures. Parameters of the structure: $E_v=50$ meV, $L_b=220$ Å, unstrained barrier material, $x_{Mn}=0.045$, $x_{Mg}=0.12$. Curves are calculated. Open squares: experimental data after Ref. 6.

netic quantum numbers. Moreover, the weighting factors depend strongly on the magnetic field, which is shown in Fig. 4. In each diagram, only the weighting factors of the $|F^k_{3/2}(z)|^2$ (thick line) and $|F^k_{1/2}(z)|^2$ (thin line) components are presented since it holds the relation $|F^k_{-3/2}(z)|=|F^k_{3/2}(z)|$ and $|F^k_{-1/2}(z)|=|F^k_{1/2}(z)|$, which is a consequence of the symmetry of the Hamiltonian and the symmetry of the transfer matrix. It holds, however, only in the special cases of Faraday and Voigt configurations. In tilted field configurations all weighting factors are different from each other. Comparing Figs. 2 and 3, one can see that all of the features, typically, for the magnetic field dependence of the splitting pattern of the valence-band complex, are reproduced in the experimentally observed field dependence of the optical transitions.

Thus, the anisotropy of the splitting pattern can be fully explained by the mixing of the states in dependence on the orientation of the magnetic field.

For small magnetic-field strengths the Brillouin function gives a linear dependence on the magnetic field $\vec{\mathbf{B}}$ and one has $G^v_{eff,j}\sim B_S(\xi)\sim B_j$, $(j=x,y,z)$ [see Eq. (5)]. Then, the origin of the difference in the HH and LH splitting pattern in Voigt configuration $[\vec{\mathbf{B}}=(B_x,0,0)]$ can be demonstrated by simple analytical expressions, which are obtained by the diagonalization of the bulk Hamiltonian for a particular layer, when the relation $E^v_{HH}(0)-E^v_{LH}(0)=\Delta\tilde{E}\gg\Delta E_{exc}(B)$ is fulfilled.

$$E^{1,2}_{\Gamma_8,HH}(\tilde{G})\approx\Delta\tilde{E}+\frac{3}{4}\frac{\tilde{G}^2}{\Delta\tilde{E}\mp\tilde{G}}+\cdots,$$

$$E^{3,4}_{\Gamma_8,LH}(\tilde{G})\approx\pm\tilde{G}-\frac{3}{4}\frac{\tilde{G}^2}{\Delta\tilde{E}\mp\tilde{G}}+\cdots, \qquad (15)$$

with $\tilde{G}=G^v_{eff,x}\sim B_x$. In the first approximation, the magnitude of splitting of the LH and HH doublets depend linearly and quadratically on B_x, respectively. Furthermore, the LH splitting is enhanced by a factor of 2 in comparison to Faraday configuration. The HH splitting is nonlinear and smaller than the LH splitting value.

The same mechanism can be found in SL's of opposite type where the wells consist of DMS material and the barriers are nonmagnetic. For such samples, Kuhn-Heinrich *et al.*[6] reported a strong dependence of the anisotropy of Zeeman splitting on the well width. Even this result can be explained by the present model. In Fig. 5 the dependence of the magneto-optical anisotropy on the well width L_w of $Cd_{1-x}Mn_xTe/Cd_{1-y}Mg_yTe$ SL's (Ref. 6) consisting of semimagnetic wells and nonmagnetic barriers is shown. The anisotropy has been defined as the difference $E^{Far}_{HH1}-E^{Voi}_d$ for a given field strength, where E^{Far}_{HH1} is the lowest exciton state in Faraday configuration (σ^+ polarization) and E^{Voi}_d is the lowest exciton state in Voigt configuration. The curves are calculated for unstrained barriers ($\epsilon_b=0$) and tensile or compressive strain in the well, $\epsilon_w>0$ and $\epsilon_w<0$, respectively. For $L_w\to 0$, the anisotropy must vanish since only one light- and one heavy-hole state remain in the well and both are pinned at the upper edge of the well. Thus their energetical separation tends to zero. The anisotropy also vanishes for $L_w\to\infty$ in case of $\epsilon_w=0$ since we then reach the limiting case of the bulk which is isotropic in the strain free case. For $\epsilon_w\neq 0$ the anisotropy reduces for $L_w\to\infty$ to the strain-induced part, which can be even negative for $\epsilon_w<0$. Consequently, for intermediate well width a maximum can be expected. We find that the position of the maximum is almost unchanged by the strain. The experimental values reported in Ref. 6 are in good agreement with the theoretical calculations if we assume a weak biaxial tensile strain in the wells as it was also claimed by the authors.

Finally, we demonstrate the anisotropy on an SQW for tilting angle different from Faraday ($\Phi=0°$) and Voigt ($\Phi=90°$) configurations. Changing the angle from $\Phi=0°$ to $\Phi=90°$ we found a continuous change of the splitting in dependence on the tilt. As an example in Fig. 6 the valence-

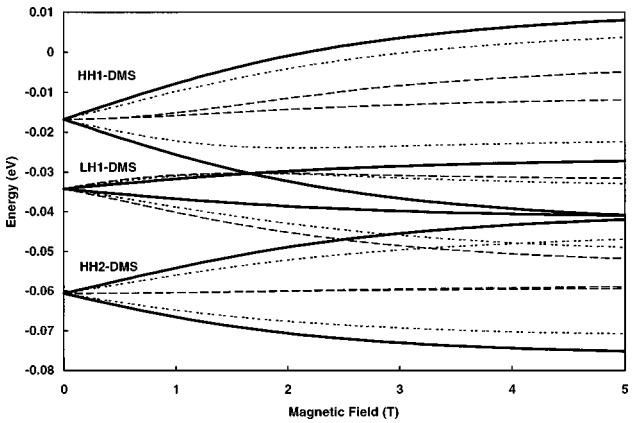

FIG. 6. Zeeman splitting pattern of the valence band states of a $Cd_{1-x}Mn_xTe/Cd_{1-x}Mg_xTe$ SQW structure in dependence on the on angle Φ between sample axis and the magnetic-field direction: valence-band offset $E_v=80$ meV, well width $L_w=45$ Å, unstrained well and barrier material, $x_{Mn}=0.045$, $x_{Mg}=0.12$. Full lines–$\Phi=0°$ (Faraday configuration), dotted lines–$\Phi=45°$, dashed lines–$\Phi=90°$ (Voigt configuration).

band Zeeman splitting is depicted for an angle of $\Phi=45°$ (dotted lines) together with $\Phi=0°$ (field along [001], Faraday configuration, full lines) and $\Phi=90°$ (field along [110], Voigt configuration, dashed lines). The energetic position of the well bottom at $B=0$ T is chosen to be the zero of energy. A decreasing HH splitting and an increasing LH splitting with increasing angle is seen accompanied by the appearance of the typical anticrossing features for all states. It should be mentioned that the model does not account for any anisotropy in the case of in-plane rotation of the magnetic field from [110] to $[\bar{1}10]$. There is up to now no experimental indication for an anisotropic behavior of DMS in dependence on the in-plane angle of the magnetic field, as was recently reported for diamagnetic ZnSe.[21]

B. Asymmetric double quantum wells

Asymmetric double-quantum-well structures are known to be excellent tools for studying tunneling processes. In particular, semimagnetic ADQW's enable the variation of the separating potential in one and the same sample, just by varying the external magnetic field (see Ref. 22 and references therein). The strong magneto-optical anisotropy should even have an impact on the tunneling properties in ADQW's consisting of DMS materials. Up to now, however, these effects have not yet been considered. In the following we discuss the magneto-optical anisotropy of such ADQW's. The exact characterization of the exciton states and their dependence on the magnetic-field orientation is a first and important step towards the description and understanding of the tunneling processes under the influence of an external magnetic field with respect to its orientation and strength.

CdTe and ZnSe based ADQW's have been fabricated by MBE containing either a semimagnetic 6-nm $Zn_{1-x-y}Cd_yMn_xSe$ well and a 6-nm $Zn_{1-x}Cd_xSe$ well, which are coupled via a 6-nm ZnSe barrier or two CdTe wells with widths of 4 and 8 nm coupled via $Cd_{1-x}Mn_xTe$ barriers of different thicknesses. The ZnSe based ADQW's have been grown on (100) GaAs substrates and the CdTe

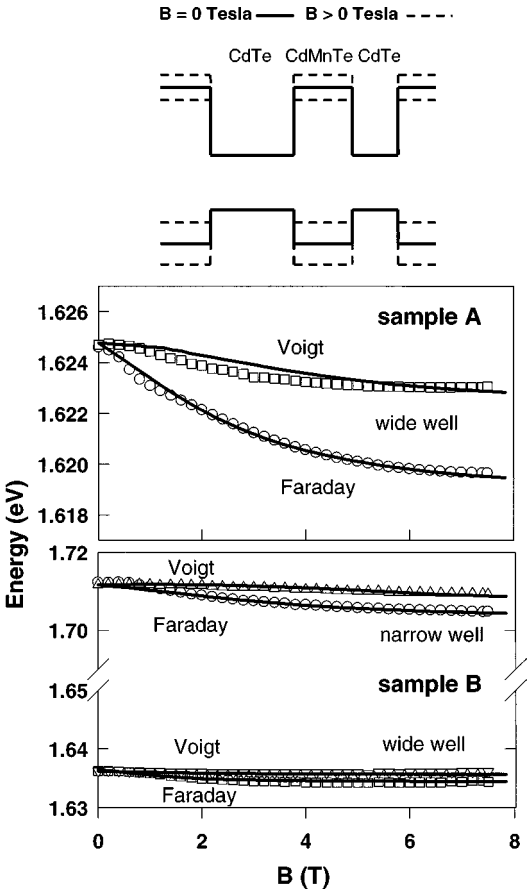

FIG. 7. Energetic position of the excitonic PL (symbols) in dependence on the magnetic field strength for $CdTe/Cd_{1-x}Mn_xTe$ ADQW structures for $\mathbf{B}\|\mathbf{z}$ (Faraday) and $\mathbf{B}\perp\mathbf{z}$ (Voigt). $T=1.8$ K, $E_{ex}=2.820$ eV. Curves are calculated. The schematic diagram shows the band structure of the ADQW at zero field (full lines) and at an elevated field strength (dashed lines).

based ADQW's have been grown on (100) InSb substrates. In the case of $CdTe/Cd_{1-x}Mn_xTe$-ADQW's the asymmetry of the samples is given by different CdTe well widths (see top of Fig. 7). The giant Zeeman splitting occurs primarily only in the barriers as these are made of $Cd_{1-x}Mn_xTe$ (sample A: $x_{Mn}=0.08$; sample B: $x_{Mn}=0.16$). As a consequence a reduced shift and splitting is found for the nonmagnetic well states, which can be considered to be caused by the change of the barrier height. In the case of $Zn_{1-x-y}Cd_yMn_xSe/ZnSe$-ADQW's the asymmetry is given by different well depths (see top of Fig. 8). The barriers are made of nonmagnetic ZnSe. One semimagnetic well ($Zn_{1-x-y}Mn_xCd_ySe$; sample C: $x_{Mn}=0.18$, $y_{Cd}=0.11$ and sample D: $x_{Mn}=0.15$, $y_{Cd}=0.09$) has been prepared for each sample, whereas the second well ($Zn_{1-y}Cd_ySe$) is nonmagnetic and does not exhibit, therefore, an inherent giant Zeeman splitting.

In the low-temperature photoluminescence (PL) usually only the lowest-energy exciton transition can be observed due to thermal equilibrium. For samples C, D and particularly B, however, both wells are strongly separated (due to the thickness and height of the inner barrier) and, therefore, PL from either well is found. In Figs. 7 and 8 the PL shifts are depicted for all ADQW's as a function of the magnetic-field strength with $\vec{\mathbf{B}}\|\mathbf{z}$ and $\vec{\mathbf{B}}\perp\mathbf{z}$. A stronger shift to lower

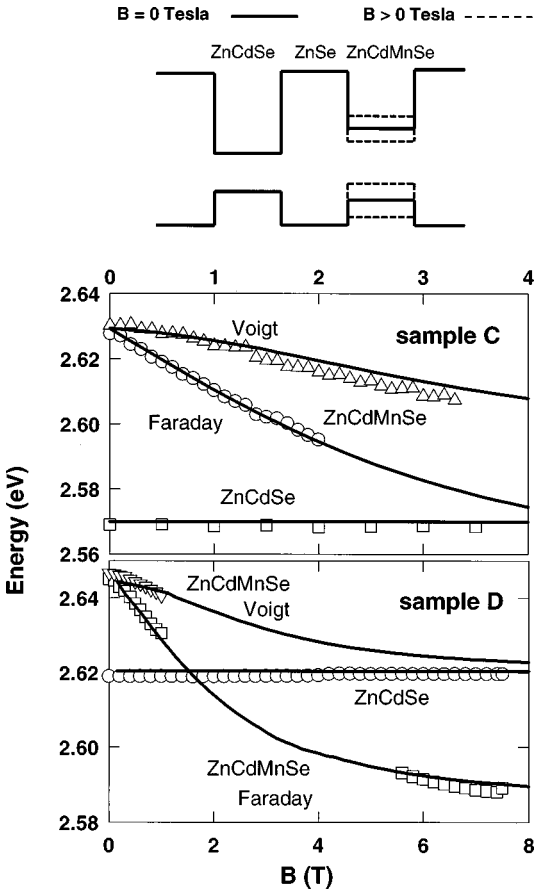

FIG. 8. Energetic position of the excitonic PL (symbols) in dependence on the magnetic-field strength for $Zn_{1-y}Cd_ySe/ZnSe/Zn_{1-x-y}Cd_yMn_xSe$ ADQW structures for $\mathbf{B}\|\mathbf{z}$ (Faraday) and $\mathbf{B}\perp\mathbf{z}$ (Voigt). $T=1.8$ K, $E_{ex}=2.820$ eV. Curves are calculated. The upper diagram shows the schematic band structure of the ADQW at zero field (full lines) and at an elevated field strength (dashed line).

energies with increasing field is always found in Faraday configuration compared to Voigt configuration. It can be seen from Figs. 7 and 8 that the PL bands are always lower for $\vec{\mathbf{B}}\|\mathbf{z}$ compared to $\vec{\mathbf{B}}\perp\mathbf{z}$. Such is the predicted behavior (on the basis of the theory discussed above) if the HH exciton is the lowest-energy transition at zero field. As the wells are under compressive strain this is valid for all specimens discussed here. The sequence is inverted if the LH is the ground state at zero field.[4]

In the case of ZnSe based ADQW's (Fig. 8), the giant Zeeman effect and a strong anisotropy are seen for the DMS wells as expected, but no shifts are observable for the nonmagnetic $Zn_{1-x}Cd_xSe$ wells, as there is no interaction of the corresponding exciton states with the Mn ions of the adjacent well.

We have to mention here, that the magnetic-field-induced mixing of the valence-band states takes place always if the T_d symmetry is reduced and the symmetry axis is tilted against the field direction, even in the case of nonmagnetic semiconductors, but the corresponding very small energy shift and splitting which are observable, e.g., in spin-flip Raman measurements[21] are far beneath the exciton linewidths of our semimagnetic QW structures and, therefore, not observable in our experiments. The curves in Figs. 7 and 8 are calculated. The Stokes shifts were taken from the experiments and are included to account for the difference between the PL and the PLE bands at zero fields. As can be seen again a good coincidence with the experimental points has been achieved. In Fig. 9 the results of PLE measurements of sample C are depicted. More exciton states become observable now, but not all transitions are allowed in Faraday configuration. In Voigt configuration, in principal, all transitions should be observable due to the valence-band mixing. In Fig. 9 only the best detectable transitions (symbols) are compared

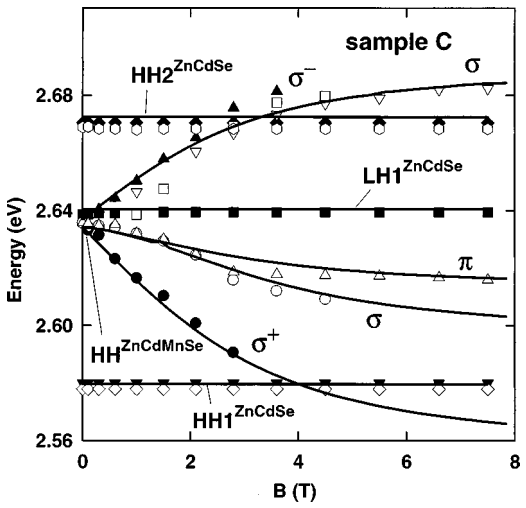

FIG. 9. Energetic position of the measured PLE bands of sample C (see Fig. 8) in dependence on the magnetic-field strength (symbols) for $\mathbf{B}\|\mathbf{z}$ in σ^+ and σ^- polarization and $\mathbf{B}\perp\mathbf{z}$ in σ and π polarization. $T=1.8$ K. Curves are calculated.

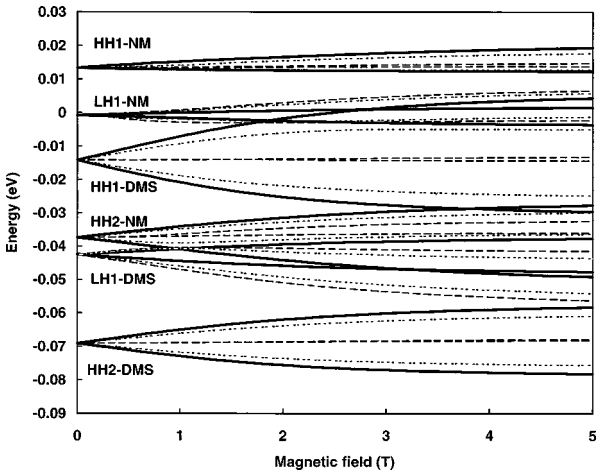

FIG. 10. Zeeman splitting pattern of the valence-band states for an ADQW in dependence on the magnetic-field strength for three different orientations of the magnetic field. Parameters (see Fig. 6 for DMS well): barrier width $L_b=20$ Å; well 2 nonmagnetic material, well width $L_{w2}=45$ Å, valence-band offset $\Delta E_{v2}=110$ meV. Faraday configuration ($\vec{\mathbf{B}}\|\mathbf{z}$, $\Phi=0°$), full lines. Voigt configuration ($\vec{\mathbf{B}}\perp\mathbf{z}$, $\Phi=90°$), dashed lines. Tilted field configuration $\Phi=45°$, dotted lines. The different observed states are indicated as HH L (K) and LH L (K), where $K=$DMS, NM labels the type of the well material and L denotes the ground state ($L=1$) and the first excited HH and LH states ($L=2$), respectively.

with the theoretical calculations (curves). Again a good coincidence between the experimental results and our theoretical model has been obtained.

Finally, we discuss DMS ADQW structures in a tilted field configuration. The calculated valence-band splitting pattern of an ADQW is shown in Fig. 10. The structure consists of a magnetic and a nonmagnetic well separated by a nonmagnetic barrier and have been generated by adding a nonmagnetic well (NMW) to the DMS SQW considered in Fig. 6. The NMW is 30 meV deeper than the DMS well. So we find additional states emerging from the nonmagnetic well. In contrast to the wide barrier case discussed in Fig. 8 now a thin inner barrier of only 20 Å was chosen. Therefore, we observe even for the new states of the nonmagnetic well a pronounced Zeeman splitting due to the coupling of both wells through the thin barrier. But, the presence of the nonmagnetic well modifies also the states originating from the magnetic well. The states are shifted with respect to its previous position and the magnitude of the splitting decreases in comparison to Fig. 6, because the wave functions get more delocalized by adding the nonmagnetic well and, therefore, the exchange interaction with the localized Mn^{2+} spins is reduced. For all HH states (localized either in the nonmagnetic or DMS well) a decrease of the splitting by changing the tilting angle from Faraday configuration to Voigt configuration accompanied by anticrossing is now clearly to be seen. Thus, we can conclude that the splitting pattern is characterized again by the magnetic-field-dependent mixing of the valence-band wave functions as already found for SL's and MQW's.

V. CONCLUSIONS

We studied the magneto-optical anisotropy on various types of dimensionally reduced DMS heterostructures experimentally and theoretically for orientations of the magnetic field, both in Faraday and Voigt configurations. All typical features of the experimentally observed giant Zeeman splitting and anisotropy could be explained by our theoretical model, which enables the calculation of any particularly designed quasi-2D structures for arbitrary orientations of the magnetic field. The fundamental mechanism is the mixing of HH and LH valence-band states by the in-plane component of the magnetic field in a tilted field configuration. Only in a pure Faraday configuration a coupling of the states is missing. In particular, we were able to fit all the experimental splitting patterns in Voigt and Faraday configurations of $CdTe/Cd_{1-x}Mn_xTe$, $Zn_{1-y-x}Cd_yMn_xSe/ZnSe$ and $Cd_{1-x}Mn_xTe/Cd_{1-y}Mg_yTe$ QW structures just by changing the magnetic-field direction using one and the same set of basic function. Our approach provides a basis for the unified description of quite different structures and of arbitrary orientations of the magnetic field on equal footing, which allows us to avoid special assumptions for particular structures that have been made in the approaches used until now.

[1] J. K. Furdyna, J. Appl. Phys. **65**, R29 (1988).

[2] O. Goede and W. Heimbrodt, Phys. Status Solidi B **146**, 11 (1988).

[3] E. Vornberger, W. Ossau, A. Waag, R. N. Bicknell–Tassius, and G. Landwehr, in *Physics of Semiconductors: Proceedings of the XX International Conference*, edited by E. M. Anastassakis and J. D. Joannopoulos (World Scientific, Singapore, 1990).

[4] O. Goede, W. Heimbrodt, Th. Koepp, H.-E. Gumlich, and B. Lunn, J. Cryst. Growth **117**, 886 (1992).

[5] P. Peyla, A. Wasiela, Y. Merle d'Aubigné, D. E. Ashenford, and B. Lunn, Phys. Rev. B **47**, 3783 (1993).

[6] B. Kuhn-Heinrich, W. Ossau, E. Bangert, A. Waag, and G. Landwehr, Solid State Commun. **91**, 11 (1994).

[7] J. Kossut, in *Semiconductors and Semimetals*, edited by R. K. Willardson and A. C. Beer (Academic, New York, 1988), Vol. 25, p. 183.

[8] N. B. Brandt and V. V. Moshalkov, Adv. Phys. **33**, 193 (1984).

[9] G. Bastard, Phys. Rev. B **24**, 5693 (1981).

[10] M. Altarelli, Phys. Rev. B **28**, 842 (1983).

[11] L. R. Ram-Mohan, K.-H. Yoo, and R. L. Agarwal, Phys. Rev. B **38**, 6151 (1988).

[12] B. Chen, M. Lazzouni, and L. R. Ram-Mohan, Phys. Rev. B **45**, 1204 (1992).

[13] A. Wasiela, P. Peyla, Y. Merle d'Aubigné, J. E. Nicholls, D. E. Ashenford, and B. Lunn, Semicond. Sci. Technol. **7**, 571 (1992).

[14] D. S. Chemla, Helv. Phys. Acta **56**, 607 (1983).

[15] P. Lawaetz, Phys. Rev. B **4**, 3460 (1971).

[16] G. Beni and T. M. Rice, Phys. Rev. B **18**, 768 (1978).

[17] J. A. Gaj, R. Planel, and G. Fishman, Solid State Commun. **29**, 435 (1984).

[18] R. P. Leavitt and J. W. Little, Phys. Rev. B **42**, 11 774 (1990).

[19] W. Heimbrodt, O. Goede, V. Weinhold, K. Hieke, M. Happ, N. Hoffmann, J. Griesche, and K. Jacobs, J. Lumin. **60-61**, 344 (1994).

[20] W. Heimbrodt, O. Goede, V. Weinhold, M. Happ, R. Knoch, K. Hieke, N. Hoffmann, J. Griesche, K. Jacobs, F. Neugebauer, D. Suisky, and J. Roeseler, J. Cryst. Growth **138**, 601 (1994).

[21] W. Heimbrodt, C. L. Orange, D. Wolverson, J. J. Davies, K. Kimura, and T. Yao, Phys. Rev. B **56**, 6889 (1997).

[22] K. Hieke, W. Heimbrodt, Th. Pier, H.-E. Gumlich, W. W. Rühle, J. E. Nicholls, and B. Lunn, Mater. Sci. Forum **182-184**, 587 (1995).